HAL
open science

Inland water greenhouse gas budgets for RECCAP2: 2 Regionalization and homogenization of estimates following the RECCAP2 framework

Ronny Lauerwald, George Allen, Bridget Deemer, Shaoda Liu, Taylor Maavara, Peter Raymond, Lewis Alcott, David Bastviken, Adam Hastie, Meredith Holgerson, et al.

To cite this version:

Ronny Lauerwald, George Allen, Bridget Deemer, Shaoda Liu, Taylor Maavara, et al.. Inland water greenhouse gas budgets for RECCAP2: 2 Regionalization and homogenization of estimates following the RECCAP2 framework. Global Biogeochemical Cycles, 2023, 37 (5), 10.1029/2022GB007658 . hal-04205172

HAL Id: hal-04205172

https://hal.inrae.fr/hal-04205172v1

Submitted on 12 Sep 2023

HAL is a multi-disciplinary open access archive for the deposit and dissemination of scientific research documents, whether they are published or not. The documents may come from teaching and research institutions in France or abroad, or from public or private research centers.

L'archive ouverte pluridisciplinaire **HAL**, est destinée au dépôt et à la diffusion de documents scientifiques de niveau recherche, publiés ou non, émanant des établissements d'enseignement et de recherche français ou étrangers, des laboratoires publics ou privés.

Inland water greenhouse gas budgets for RECCAP2: 2 Regionalization and homogenization of estimates following the RECCAP2 framework

Ronny Lauerwald[1], George H. Allen[2], Bridget R. Deemer[3], Shaoda Liu[4,5], Taylor Maavara[4,6], Pete Raymond[4], Lewis Alcott[7], David Bastviken[8], Adam Hastie[9], Meredith A. Holgerson[10], Matthew S. Johnson[11], Bernhard Lehner[12], Peirong Lin[13], Alessandra Marzadri[14], Lishan Ran[15], Hanqin Tian[16], Xiao Yang[17], Yuanzhi Yao[18], Pierre Regnier[19]

[1]Université Paris-Saclay, INRAE, AgroParisTech, UMR ECOSYS, Palaiseau, France

[2]Department of Geosciences, Virginia Tech, VA, USA

[3]U.S. Geological Survey, Southwest Biological Science Center, Flagstaff AZ, USA

[4]Yale School of the Environment, Yale University, New Haven, CT, USA

[5]State Key Laboratory of Water Environment Simulation, School of Environment, Beijing Normal University, Beijing, 100875 China

[6]School of Geography, University of Leeds, Leeds, LS2 9JT, UK

[7]Department of Earth & Planetary Sciences, Yale University, New Haven, CT, USA

[8]Department of Thematic Studies - Environmental Change, Linköping University, Linköping, Sweden

[9]School of GeoSciences, University of Edinburgh, Edinburgh, UK

[10] Department of Ecology and Evolutionary Biology, Cornell University, Ithaca, NY, USA

[11]Earth Science Division, NASA Ames Research Center, Moffett Field, CA, USA

[12]Department of Geography, McGill University, Montreal, H3A 0B9, QC, Canada

[13]Institute of Remote Sensing and GIS, School of Earth and Space Sciences, Peking University, China

[14] University of Trento, Department of Civil, Environmental and Mechanical Engineering, Trento, Italy

[15]Department of Geography, The University of Hong Kong, Pokfulam Road, 999077, Hong Kong, China

[16]Schiller Institute for Integrated Science and Society, Department of Earth and Environmental Sciences, Boston College, Chestnut Hill, MA, USA;

[17]Southern Methodist University, Department of Earth Sciences, Dallas, TX-75275, USA

[18]School of Geographic Sciences, East China Normal University, Shanghai 200241, China

[19]Department Geoscience, Environment & Society - BGEOSYS, Université Libre de Bruxelles, 1050 Bruxelles, Belgium

Keypoints

We synthesized estimates of river, lake and reservoir emissions of CO_2, CH_4 and N_2O for 10 world regions and globally

We re-estimate global inland water emission of 5.6 (3.5-9.1) Pg CO_2 yr^{-1}, 101 (83-135) Tg CH_4 yr^{-1}, and 326 (254-592) Gg N_2O yr^{-1}

At 20 year horizon, flowing and standing water bodies, as well as CO_2 and CH_4, contribute equally to global warming potential of emissions

Abstract

Inland waters are important sources of the greenhouse gasses (GHGs) carbon dioxide (CO_2), methane (CH_4) and nitrous oxide (N_2O) to the atmosphere. In the framework of the 2nd phase of the REgional Carbon Cycle Assessment and Processes (RECCAP-2) initiative, we synthesize existing estimates of GHG emissions from streams, rivers, lakes and reservoirs, and homogenize them with regard to underlying global maps of water surface area distribution and the effects of seasonal ice cover. We then produce regionalized estimates of GHG emissions over 10 extensive land regions. According to our synthesis, inland water GHG emissions have a global warming potential of an equivalent emission of 13.6 (10.0-20.3) and 8.3 (5.8-12.7) Pg CO_2-eq. yr^{-1} at a 20 and 100 year horizon (GWP_{20} and GWP_{100}), respectively. Contributions of CO_2 dominate GWP_{100}, with rivers being the largest emitter. For GWP_{20}, lakes and rivers are equally important emitters, and the warming potential of CH_4 is more important than that of CO_2. Contributions from N_2O are about two orders of magnitude lower. Normalized to the area of RECCAP-2 regions, S-America and SE-Asia show the highest emission rates, dominated by riverine CO_2 emissions.

1 Introduction

As part of the first phase of the REgional Carbon Cycle Assessment and Processes (RECCAP) initiative (RECCAP-1), Raymond et al. (2013) re-estimated global inland water CO_2 evasion and presented the first ever maps of CO_2 emissions from streams and rivers as well as from lakes and reservoirs. Moreover, Raymond et al. demonstrated that inland water emissions have long been underestimated (e.g. Cole et al. 2007, Aufdenkampe et al. 2011) because small water bodies, which contribute over-proportionally to the overall emission flux, had been excluded. This publication became a milestone in the field, as it demonstrated the importance of inland waters for the global C budget.

Since RECCAP1, a growing number of global estimates of inland water greenhouse gas (GHG) emissions have been published, not only for CO_2 emissions (e.g. Holgerson & Raymond, 2016; Horgby et al., 2019; Lauerwald et al., 2015; Liu et al., 2022), but also for CH_4 (e.g. Holgerson & Raymond, 2016; Rosentreter et al., 2021; Stanley et al., 2016) and N_2O (e.g. Hu et al., 2016; Lauerwald et al., 2019; Maavara et al., 2019; Marzadri et al., 2021; Soued et al., 2016; Yao et al., 2020), or for all three GHGs combined (e.g. Deemer et al., 2016; DelSontro et al., 2018). More importantly, global scale estimation of inland water GHG budgets have been improved through novel upscaling techniques based on statistical (e.g. Lauerwald et al. 2015, DelSontro et al. 2018, Liu et al. 2022) and process based models of varying complexity (e.g. Maavara et al. 2019, Yao et al. 2020). These upscaling techniques have been used to create gridded global maps of inland water emissions that allowed for the inclusion of inland waters in improved and spatially disaggregated, global GHG budgets (Bastos et al., 2020; Ciais et al., 2021; Stavert et al., 2022; Tian et al., 2020). However, previously published datasets and estimates differ largely with regard to the total global water surface area, which has been identified as one of the major persisting sources of uncertainties in global estimates of inland water GHG emissions (DelSontro et al. 2018). In a companion paper (Lauerwald et al., submitted), we review these global estimates of inland water GHG emissions in detail.

Here, in the framework of the second phase of RECCAP (RECCAP-2), we present a synthesis of inland water GHG emissions based on these global estimates. Consistent with the overall objective of RECCAP-2 (Ciais et al., 2022), our synthesis covers inland water emissions of CO_2, CH_4, and N_2O and breaks down existing estimates over 10 major world regions: North America (N-America), South America (S-America), Europe, Africa, Russia, West Asia (W-Asia), East Asia (E-Asia), South Asia (S-Asia), South-East (SE-Asia) and Australasia. Inland waters included in our synthesis comprise streams and rivers, as well as lakes and reservoirs. Note that smaller lentic water bodies such as ponds are not included in the synthesis due to lack of data regarding their global distribution. Further, temporally inundated floodplains and swamps are not included here, as those are wetlands which should be considered distinct from inland waters in GHG budgets.

We strive to give reasonable ranges of emission estimates at the global scale and for the 10 regions used in RECCAP-2, homogenizing existing estimates with regard to the assumed effective inland water surface area. For this, we make use of the most up-to-date datasets of inland water surface areas and estimates of seasonal ice-cover (section 2). Then, based on existing estimates and collections of published, observed emission rates (as reviewed in Lauerwald et al.,submitted), we re-estimate the total emission

of CO_2 (section 3), CH_4 (section 4), and N_2O (section 5) per type of inland water and per RECCAP-2 region. Finally, we present the full inland water GHG budget in terms of total warming potential at a 20 and 100 year time horizon (section 6).

2 Homogenization of existing estimates

For our regionalized synthesis of inland water GHG emissions, we selected the most appropriate existing global estimates, complemented by a few regional assessments where appropriate (see details in sections 4-6, and Lauerwald et al. submitted). As mentioned before, we rescaled those estimates to consistent values of inland water surface area, accounting for the effects of seasonal ice-cover. In the following, we briefly describe the general methodology applied for this synthesis, starting with the general strategies to calculate area-normalized GHG flux rates for each estimate and RECCAP-2 region (2.1). Then we describe the selected datasets of inland water surface areas that were applied for this synthesis (2.2), and how we corrected for effects of seasonal ice cover (2.3).

2.1 Calculation of area-normalized fluxes

Area-normalized fluxes were calculated in different ways, depending on the upscaling approach employed by each original study. For estimates based on direct empirical upscaling, where a global mean areal flux was applied to a global water surface area, the same areal flux was applied here to each of the 10 RECCAP-2 regions, multiplying by the water surface area used in this synthesis. For binned upscaling, where this form of upscaling was performed for individual waterbody size classes (e.g. Holgerson and Raymond 2016; Rosentreter et al. 2021) or latitude bins (e.g. Bastviken et al. 2011, Rosentreter et al. 2021, Harrison et al. 2021, Marzadri et al. 2021), the same bins were used, multiplying originally reported mean areal fluxes by the surface area of each bin calculated in this study. Finally, spatially explicit estimates of areal GHG fluxes (as for instance Stavert et al. 2022 and Johnson et al. 2021) were averaged by RECCAP-2 region, and then multiplied by the surface area used for our synthesis. However, where GHG emissions are simulated with process-based, biogeochemical models, emission estimates scale to simulated biogeochemical transformation fluxes and are rather independent of the assumed water surface area (see for instance Lauerwald et al. 2017). This is the case for model based estimates of N_2O (Yao et al. 2020, Maavara et al. 2019, Lauerwald et al. 2019) and CO_2 (Tian et al. 2015). Here, we aggregated the original flux estimates directly per RECCAP-2 region. Details on which estimates were used for our regionalized synthesis, and which type of areal-homogenization was applied is given in the following three sections for CO_2 (3), CH_4 (4), and N_2O (5).

2.2 Water surface data used in this synthesis

For rivers, the primary source of surface area comes from the GRWL database v.1.0 (Allen & Pavelsky 2018) (Figure 1a), which we consider the best-available dataset for that purpose (see, Lauerwald et al., submitted for further details). Following the approach presented in Allen & Pavelsky (2018), we calculate the total global river surface area as 773,000 km^2, excluding the effects of seasonal ice cover. In this approach, the surface area of rivers and streams narrower than 90 m was estimated by developing basin-specific statistical distributions of river widths in large rivers and extrapolating these widths to

narrower rivers and streams (Allen & Pavlesky, 2018). As seen in Figure 1a, a large amount of river surface area is concentrated in the tropics and the Arctic, particularly if the impact of river ice is not taken into consideration.

For lake and reservoir surface area, we use data from HydroLAKES v.1.1 (Messager et al., 2016). HydroLAKES contains only water bodies larger than 0.1 km^2 and is thus rather conservative with regard to total lake and reservoir surface area. We prefer these rather conservative estimates over remote-sensing based products (e.g. GloWaBo by Verpoorter et al. 2014) which may be contaminated with wrongly attributed surface areas, in particular as non-supervised classification algorithms have been applied. More importantly, HydroLAKES classifies each water body as a natural lake, a reservoir, or a natural lake with a dam (e.g., Lake Victoria in Figure 1b). The distinction between natural lakes and reservoirs is important, as we partly deal with distinct areal flux rates for both types of standing water bodies. For each of the three lake types distinguished in HydroLAKES, we sum water surface area in each of the 10 RECCAP-2 regions (Figure 1c). Excluding the effects of ice cover and water bodies with a surface area less than 0.1 km^2, the total surface area of natural lakes is 2,442,443 km^2, reservoirs is 266,894 km^2, and lakes with a dam is 209,474 km^2, for a grand total of 2,918,811 km^2.

Some of the GHG emission estimates we synthesized give estimates per latitudinal bands and/or per stream order (see section 3 to 5). To provide useful input for rescaling those estimates to the river surface area used for this study, we partitioned the stream surface area accordingly. For stream order, we determine the surface area of rivers and streams with a Horton-Stahler stream order ≤3 and stream order >3. To accomplish this task, we use the HydroSHEDS-based RiverATLAS version 1.0 dataset (Linke et al., 2019), which contains the stream order and an estimated river surface area for each river segment based on hydraulic geometry relationships from Allen et al. (1994). For each RECCAP-2 region, we calculate the proportion of surface area of rivers and streams in RiverATLAS in each stream order category and then apply this proportion to the surface area of each RECCAP-2 region derived from Allen & Pavelsky (2018). Estimates of areal proportions of different lake size classes were obtained based on the attribute data stored in the HydroLAKES v.1.1 database.

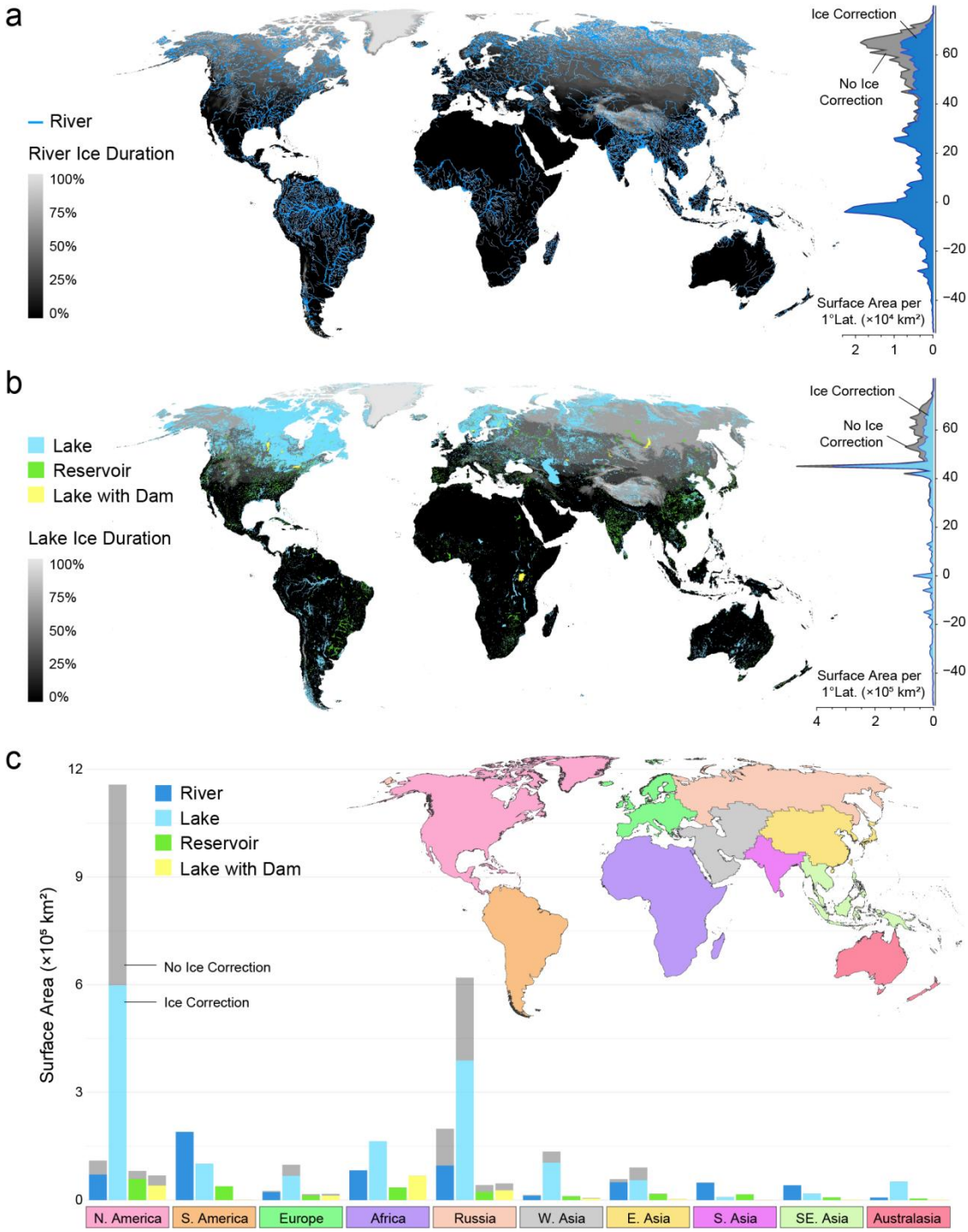

Figure 1. Global surface area of inland water bodies. a) River surface area with ice duration correction. b) Lake, Reservoir, and Lake with dam surface area with ice duration correction. c) Water body surface area within each of the 10 RECCAP-2 regions. Insets in panels a and b report the latitudinal distribution of water surface area without / with ice correction.

2.3 Correction for effects of ice-cover

We account for the effects of river ice by reducing the amount of river surface area by the proportion of the year that rivers are covered by ice (Figure 1a). We estimate ice duration using the river ice model presented by Yang et al. (2020). The model uses a logistic regression equation to estimate river ice probability from the mean surface air temperature and considers the difference between freeze-up and breakup processes. Surface air temperature inputs to the river ice model are from ERA5 climate reanalysis daily aggregated data from 2010-07 to 2020-07 (https://cds.climate.copernicus.eu/). Each daily probability ([0–1]) map is then converted to binary "ice-cover" (≥0.5) or "ice-free" (<0.5) map, before all the daily binary rasters are temporally averaged across the 10-year study period to arrive at the 10-year river ice occurrence raster (Figure 1a). The GRWL-based river surface area measurements are then scaled by the proportion of the year that rivers are ice free. The ice correction reduces the global effective surface area of rivers and streams to 616,000 km^2 (a relative decrease of 20.3%) and is particularly important in N-America and Russia, where river ice is most prevalent (Figure 1c).

To account for the effect of ice cover on lakes and reservoirs during the winter months, we multiply the surface area of each lake and reservoir by the average proportion of the year that the waterbody remains ice free (Figure 1b). We estimate lake and reservoir ice duration using monthly surface air temperatures from 1970-2000 from WorldClim 2 (Fick & Hijmans, 2017). For each lake and reservoir, we determine the proportion of the year that surface air temperatures are below 0°C, an isothermic threshold that is a good predictor of lake ice occurrence (Murfitt & Brown, 2017; Sharma et al., 2019; Weyhenmeyer et al., 2004). Applying the ice cover correction reduces the global effective surface area of natural lakes to 1,553,842 km^2 (a relative decrease of 36.4%), reservoirs to 219,082 km^2 (17.9%), and lakes with a dam to 154,610 km^2 (26.2%), for a grand total effective surface area of 1,927,534 km^2 (34.0%). Much of this reduction occurs in natural lakes located in the Canadian Shield and in Siberia corresponding to RECCAP-2 regions N-America and Russia (Figure 1c).

Spring ice melt is associated with a pulse of CH_4 and CO_2 emissions from lakes and reservoirs (Denfeld et al., 2018). Specifically, Denfeld et al. (2018) estimates that 17% of annual emissions of carbon dioxide and 27% of annual emissions of methane occur during this ice-off period in lakes and reservoirs. Thus, for lakes and reservoirs that freeze, we applied as well a corresponding ice-melt correction factor for CO_2 and CH_4, which lowers the overall impact of seasonal ice cover. This should be noted as a simplification based on studies of a limited number of individual systems, not accounting for their representativity in terms of system characteristics or ice period length. While there is preliminary evidence that a similar ice-off flux of N_2O may take place in some northern lakes (Cavaliere & Baulch, 2018), there remains insufficient field data as well as mechanistic understanding of under-ice N_2O production processes to scale this process to any of the RECCAP-2 regions or globally. Thus, inland water N_2O emission is only corrected for by rescaling fluxes to relative length of ice-free period.

3 Inland water CO_2 budget

In our companion paper presenting a review on existing global inland water GHG budgets (Lauerwald et al. submitted), we identified global water surface area as a major factor of uncertainty explaining a large

proportion of differences between estimates. In this synthesis, we remove that factor of inconsistency and standardize all flux estimates reviewed in Lauerwald et al. (submitted) to the same dataset of inland water surface area (Allen and Pavelsky, 2018; Messager et al. 2016) and apply the same procedure of correction of seasonal ice-cover as explained in section 2.3. The rescaled emission estimates from the individual studies retained for that synthesis are listed in Table S1. Most of these estimates are global, spatially explicit estimates covering all regions (Raymond et al. 2013, Lauerwald et al. 2015, Liu et al. 2022, and simulation results from DLEM), which were complemented by regional estimates covering only one (Borges et al., 2015; Butman & Raymond, 2011; Li et al., 2018; Ran et al., 2021) or two regions (Hastie et al., 2018). For standardizing the studies by St. Louis et al. (2000), Deemer et al. (2016), and DelSontro et al. (2018) that are based on a robust database of observations but only give a lumped global estimate, we simply applied the same average emission rate to the ice-corrected water surface area of the corresponding water body type in each RECCAP-2 region. Note that following DelSontro et al. (2018), we used two average emission rates for this study, one simply based on the mean of observations, and one derived from statistical upscaling based on assumed statistical distributions of phosphorus concentrations and water body size. Using the lake size distribution from HydroLAKES, the second emission rate (277 g CO_2 $m^{-2}yr^{-1}$) based on statistical upscaling is less than half of the rate derived from the arithmetic mean of observations (615 g CO_2 $m^{-2}yr^{-1}$). Although the statistical function used by DelSontro et al. (2018) has a low R^2 of 0.11 and upscaling results are thus not necessarily robust, the large difference between both rates indicates that the observational basis is not necessarily representative for global lakes, suggesting that direct upscaling of observations might lead to strong overestimations. We thus retained both rates for our analysis, as lower and upper bound values derived from the same observational dataset, the range reflecting the huge uncertainty arising from distinct upscaling methods. For standardizing the estimates by Holgerson & Raymond (2016), we applied the reported average emission rates for four lake size classes (0.1-1 km^2, 1-10 km^2, 10-100 km^2, >100 km^2). For the estimates by Harrison et al. (2021), we used average emission rates for four latitudinal bands (0-25, 25-54, 54-66, >66 degree latitude). Figure 2 shows the ranges of all standardized estimates per water body type and RECCAP-2 region. It also reports the correction factors that were applied to account for seasonal ice cover and the emission pulse during spring ice melt.

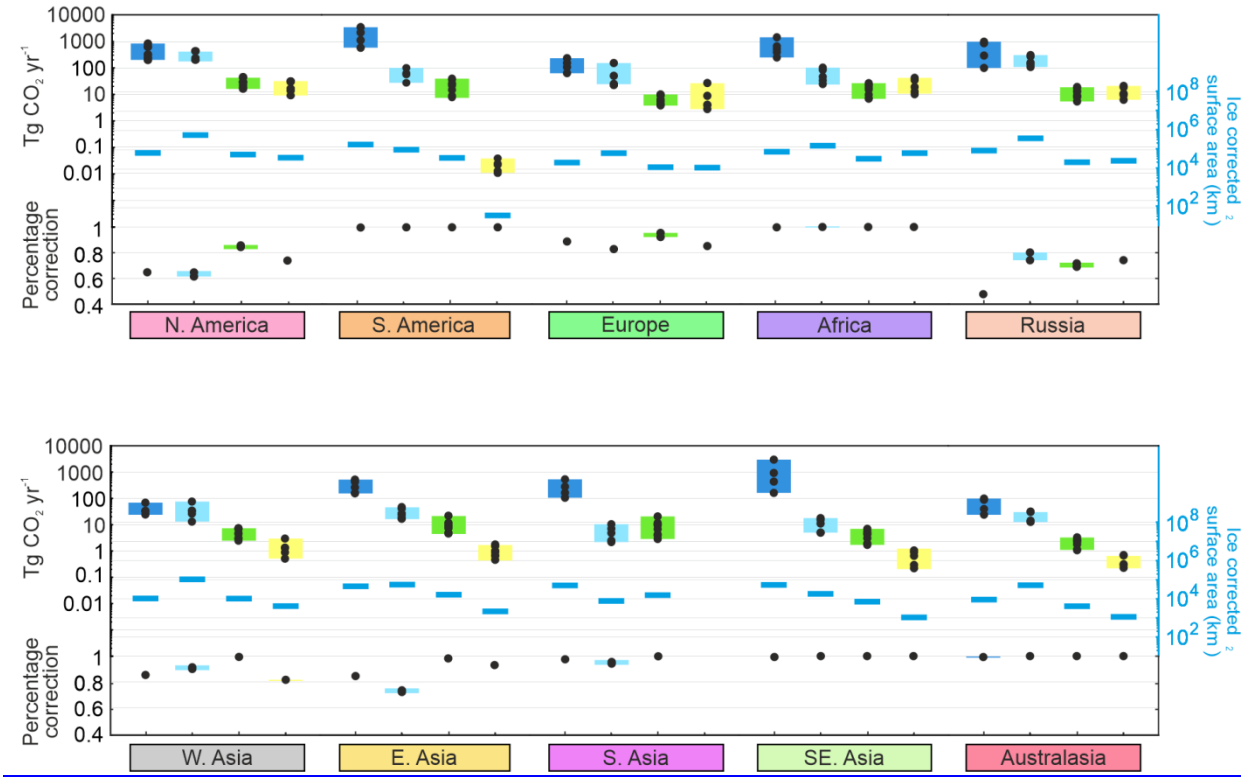

Figure 2: Spatial and statistical distribution of standardized inland water CO_2 emission flux. Regional estimates of CO_2 emission (Tg CO_2-C yr^{-1}) in the top bars, ice corrected surface area estimates in blue lines, and the percent change in total annual emission from the combination of ice and ice melt corrections in the bottom bars. Regional emissions are shown from rivers (dark blue), natural lakes (light blue), reservoirs (green) and lakes with a dam (yellow). Each black dot represents the regionalized emission from one study in the literature, such that the bars show the range of regionalized emissions across studies. More detailed information on the individual flux estimates can be found in Table S1.

If we sum up the median (min-max) values of surface-area homogenized estimates per RECCAP-2 region over the globe, we obtain CO_2 evasion fluxes of 4.49 (1.65-11.56) Pg CO_2 yr^{-1} for streams and rivers, 0.71 (range: 0.43-1.29) Pg CO_2 yr^{-1} for lakes, 0.11 (range: 0.05-0.20) Pg CO_2 yr^{-1} for reservoirs, respectively (see Table S2). Lakes regulated by dams as third lake type contribute another 0.06 (range: 0.03-0.13) Pg CO_2 yr^{-1}. When we aggregate these estimates to assess the total global inland water CO_2 emissions, we have to account for all possible combinations of individual estimates. If we sum up all median values (interquartile range) of all possible combinations per RECCAP-2 region, we calculate an emission of 5.56 (IQR: 3.51-9.10) Pg CO_2 yr^{-1}. Streams and rivers are the largest contributor to the global aquatic CO_2 evasion (~ 84%), despite a surface area of only 1/5 that of global lakes, but with average emission rates about one order of magnitude higher than those of lakes and reservoirs (see Lauerwald et al. submitted). In comparison, lakes and reservoirs make up only 13 and 2% of the total aquatic evasion, respectively. Globally, seasonal ice coverage that is partly counterbalanced by peak emissions during ice melt still removes 18% of estimated annual CO_2 emissions from inland waters. The most important reductions are estimated, not surprisingly, for Russia (46%) and N-America (35%).

Across the RECCAP-2 regions, S-America has the highest aquatic CO_2 evasion (1.72 Pg CO_2 yr^{-1}), followed by Africa, SE-Asia, Russia and N-America (0.68-0.80 Pg CO_2 yr^{-1}, all median estimates, see Table S2). In contrast, Australasia and the W-Asia have the lowest aquatic CO_2 evasion among the RECCAP-2 regions (median estimates of 0.07-0.09 Pg CO_2 yr^{-1}). In most RECCAP-2 regions, rivers are the dominant contributor to aquatic CO_2 emissions. Exceptions are N-America and W-Asia, where they contribute only half of the emissions flux, due to the fact that in these regions the inland water surface area is strongly dominated by lakes (see Figure 2). In contrast, in S-America, S- and SE-Asia, standing waters contribute less than 5% to the estimated inland water CO_2 emission.

4 Inland water CH_4 budget

In this synthesis, we calculate total area-normalized CH_4 fluxes from each study reviewed in the companion paper by Lauerwald et al. submitted, considering both diffusive and ebullitive pathways but excluding plant-mediated fluxes (as in Bastviken et al. 2011) and reservoir turbine degassing (as in Harrison et al. 2021). The individual results of this area-normalization are listed in Table S1, based on which Figure 3 gives an overview of value ranges and the effect of correction for seasonal ice-cover. However, when summarizing regionalized aquatic CH_4 emissions, we do not include emission estimates from older studies that incorporated unrealistic areal coverages and small sample sizes of observed emission rates (reservoir fluxes from St. Louis et al. 2000 and river fluxes from Bastviken et al. 2011). We also do not include studies that quantified only diffusive CH_4 fluxes and did not consider ebullition (Holgerson and Raymond 2016 and Stanley et al. 2016). These regionalized fluxes are, however, included in Figure 3 as "X" symbols. Among the studies retained for the regionalization and homogenisation of methane emission from standing water bodies, there are two studies that were based on direct upscaling (Deemer et al. 2016, DelSontro et al. 2018), four studies based on binned upscaling (Rosentreter et al. 2021, Holgerson and Raymond 2016, Harrison et al. 2021, Bastviken et al. 2011), and finally two gridded estimates (Stavert et al. 2022; Johnson et al. 2021). For rivers we only retained the estimate based on the binned upscaling by Rosentreter et al. (2021). Depending on the spatial resolution of the original studies (global, binned, regionalized, gridded), estimates were rescaled to a homogenized dataset of total and effective (i.e. corrected for effects of seasonal ice-cover and ice melt) water surface area as described in section 2. Note that for two studies (Johnson et al. 2021; Harrison et al. 2021), which included a correction of seasonal ice-cover, we were not able to disentangle the ice-correction from areal emission rates. In these two cases, instead of applying our own correction, we adopted the ice-correction from the original studies. Finally, we also included two regional estimates in our analysis: the study by Borges et al. (2015) that gives estimates for African rivers and the study by Li et al. (2018) that gives estimates for lakes and reservoirs in China. In the latter case, we extrapolated the average flux rates over the whole of RECCAP-2 region E-Asia, which besides China further includes the two Koreas and Japan.

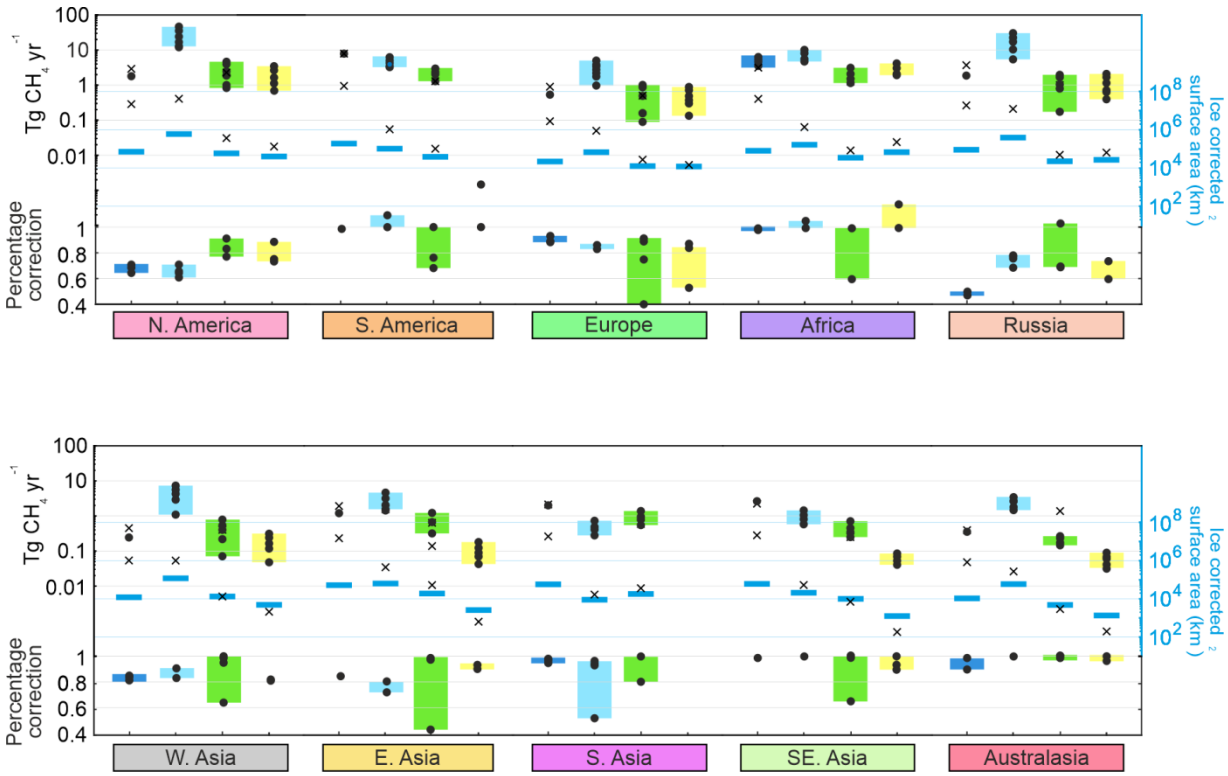

Figure 3. Spatial and statistical distribution of standardized inland water CH_4 emission flux. Regional estimates of methane emission (Tg CH_4 yr^{-1}) in the top bars, ice corrected surface area estimates in blue lines, and the percent change in total annual emission from the combination of ice and ice melt corrections in the bottom bars. Regional emissions are shown from rivers (dark blue), natural lakes (light blue), reservoirs (green) and lakes with a dam (yellow). An "X" indicates diffusive-only emission estimates. Each black dot represents the regionalized emission from one study in the literature, such that the bars show the range of regionalized emissions across studies. More detailed information on the individual flux estimates can be found in Table S1.

Aside from wetlands (not examined here), lakes are the single largest source of inland water methane emissions, emitting a median (min-max) of 59.2 (31.8-115.7) Tg CH_4 yr^{-1} followed by rivers with 22.9 Tg CH_4 yr^{-1}, and reservoirs with a median emission of 10.6 (4.8-17.8) Tg CH_4 yr^{-1} (see Table S3). Lakes with dams, which we consider here separately as a third category of standing water bodies following Messager et al (2016), contribute a median (min-max) emission of 6.2 (3.4-10.9) Tg CH_4 yr^{-1}. For standing water bodies, area-homogenisation has slightly reduced the spread in estimates from a factor 4-5 (Lauerwald et al. submitted) to a factor 3-4 (Table S3). The dominance of lake emissions is the most prominent in Regions N-America, Russia, W-Asia and Australasia where they contribute about 80% to inland water CH_4 emissions (see Figure 3 and Table S3). While the dominance of lakes in methane emissions holds for the majority of regions, the large surface area of rivers in S-America, S- and SE-Asia result in river methane emissions that rival or exceed lake emissions. In these same three regions, reservoirs constitute a high fraction of lentic water bodies (and methane emissions). Africa also has a high fraction of its freshwater methane emissions coming from lakes with a dam.

When combining these rescaled estimates to re-assess the total global inland water CH_4 emission, we have again a large number of possible combinations. If we calculate median values (and interquartile ranges - IQR) of all possible combinations of estimates covering all types of inland waters per RECCAP-2 region (see Table S3) and sum those up, we obtain a global inland water CH_4 evasion flux estimate of 100.7 (IQR: 82.6-134.7), which is at the lower end of the range of estimates reported in AR6 of the IPCC (112-217 Tg CH_4 yr^{-1}). Highest inland water CH_4 emissions of 27.5 (IQR: 19.8-41.5) and 17.7 (IQR: 13.8-29.3) Tg CH_4 yr^{-1} are estimated respectively for N-America and Russia, which together cover more than two thirds of total lake surface area. In place three and four follow the large tropical regions, Africa and S-America with 17.2 (IQR: 15.5-18.8) and 14.2 (IQR: 13.6-15.1) Tg CH_4 yr^{-1}, respectively. Together, these four regions are responsible for about three quarters of the global inland water CH_4 emissions estimated here.

Several studies have highlighted the importance of northern lakes in the global methane budget and their potential sensitivity to climate change (Wik et al. 2016). Lake-based methane emissions from N-America and Russia sum to a median emission of 41.9 (range: 23.2-76.2) Tg CH_4 yr^{-1} (Table S3), i.e. roughly about ⅔ of global lake CH_4 emissions. For comparison, Wik et al. 2016 estimate that northern lakes and ponds above 50°N emit 16.5 Tg CH_4 yr^{-1} (Wik et al. 2016). This estimate would be in line with our regional fluxes given that about 47% of our ice-corrected lake surface area in N-America, Europe and Russia is above 50 degrees latitude. A recent dataset increases the sample size of methane emissions from northern lakes and ponds but this information has not yet been upscaled (Kuhn et al., 2021).

The ice correction applied here, which incorporates both winter ice cover and additional methane flux during ice off, resulted in a reduction of global inland water CH_4 emission by 20%. Global lake CH_4 emissions are reduced by 23%, while that of rivers and reservoirs are reduced by only 12% and 17%, respectively. The higher reduction for lake emissions can easily be explained by their high abundance in boreal to arctic regions. The regions with the highest ice cover related reductions of inland water CH_4 emissions are North America (33%) and Russia (26%), where lakes dominate inland water emissions (Table S3).

5 Inland water N_2O budget

For the regionalized area-normalized reassessment of N_2O emissions from rivers, we only retained the three most recent studies reviewed by Lauerwald et al. (submitted), which provided spatially resolved estimates (Maavara et al. 2019, Yao et al. 2020, Marzardri et al. 2021, see Table S1), see our companion paper for a justification of this choice. For the regionalized reassessment of N_2O emission from lakes, we distinguished again three types of lakes from the HydroLAKES database: natural lakes, reservoirs, and lakes regulated by dams. Only two estimates reported in Lauerwald et al. (submitted) allowed to distinguish the contribution of all three lake types: the model based study by Lauerwald et al. (2019) and the direct upscaling approach after DelSontro et al. (2018). For the latter, we applied the average areal emission rate of 78.6 mg N_2O m^2yr^{-1} (DelSontro et al. 2018). Note that this emission rate was derived without separating lakes from reservoirs, and that we used this rate indistinctly to re-estimate the N_2O emissions from the three different types of lakes (natural lakes, reservoirs, lakes with dams). Lauerwald et al. (2019), on the contrary, explicitly made spatially resolved estimates for each of the three types of

lakes distinguished here. For reservoirs only, we also included the estimate based on direct upscaling from a global average N_2O emission rate of 172 mg $N_2O/m^2/yr$ reported by Deemer et al. (2016). This value was derived from observations from this specific water body type, and is about twice as high as the one after DelSontro et al. (2018). Further, we included the model-based studies by Maavara et al. (2019) and Yao et al. (2020) which give area-integrated estimates for dammed water bodies, including both reservoirs (lake types 2) and lakes regulated by a dam (lake type 3). In both cases, we used the area ratio between these two lake types to break down the merged estimates. Finally, we also added two regional estimates in our analysis: the study by Borges et al. (2015) that gives estimates for African rivers and the study by Li et al. (2018) that gives estimates for lakes and reservoirs in China. In the latter case, we extrapolated the average flux rates over the whole of RECCAP-2 region 7 (East Asia), which besides China further includes the two Koreas and Japan. The estimates after Borges et al. (2015) are quite comparable to the estimates after Maavara et al. (2019) and Marzadri et al. (2021) for African rivers (Table S1). For E-Asian standing waters, estimates after Li et al. (2018) fall in the range of the broken down global estimates for reservoirs and lakes with a dam, but are substantially higher for lakes without a dam.

Our synthesis in Figure 4 shows the range of estimates per RECCAP-2 region, homogenized with regard to inland water surface area and effects of seasonal ice-cover (see section 2). More detailed results from the statistical analysis of the rescaled emission estimates can be found in Table S4 and are discussed below. We see that after omitting the older, much higher estimates based on EF approaches (see Lauerwald et al., submitted), the spread in the estimates of inland water N_2O emissions is substantially reduced (Table S1), but even the retained, area-normalized estimates of inland water N_2O emissions still range over one order of magnitude. At global scale, the surface-area homogenized median (min-max) estimates for aquatic N_2O evasion are 130 (71-445) Gg N_2O yr^{-1} for streams and rivers, 124 (27-205) Gg N_2O yr^{-1} for lakes and 41 (16-101) Gg N_2O yr^{-1} for reservoirs, respectively. Lakes regulated by dams as a third lake type contribute another 18 (4-40) Gg N_2O yr^{-1}. If we calculate median values (and interquartile ranges - IQR) of all possible combinations per RECCAP-2 region and sum those up (as performed for CO_2 and CH_4), we obtain a global inland water N_2O evasion flux estimate of 326 (IQR: 254-592) Gg N_2O yr^{-1}. This estimate is at the far lower end of the 500-1100 Gg N_2O yr^{-1} given in AR6 of the IPCC. Our median global emission flux includes a reduction of 29% due to seasonal ice cover. Despite a surface area of only 1/5 that of global standing water bodies, streams and rivers are the largest contributor to inland water emissions (40%), followed closely by lakes which contribute another 38% of the total aquatic evasion. The most important contributors to global inland water N_2O emissions are N-America, S-America, and Africa, with median emissions of 83 (IQR: 59-107), 53 (IQR: 47-98), and 48 (IQR: 40-60) Gg N_2O yr^{-1}, respectively. These three RECCAP-2 regions account for more than half of global inland water N_2O emissions.

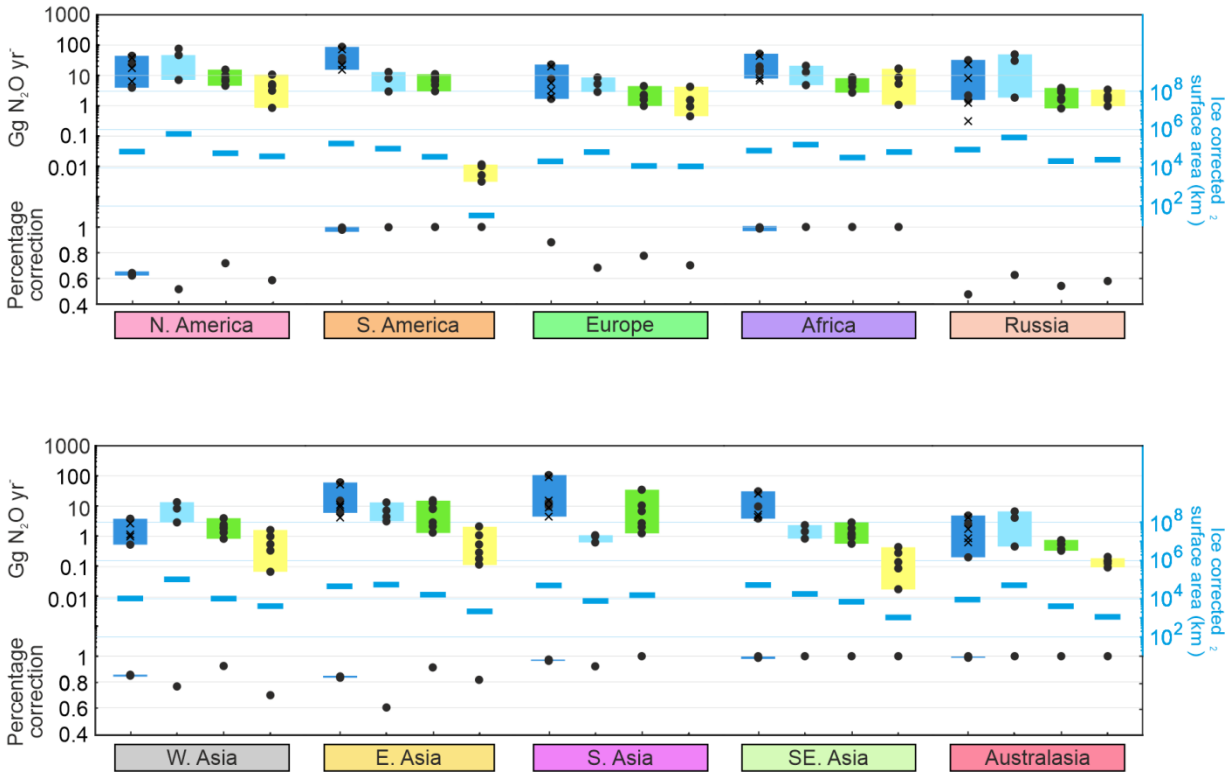

Figure 4. Spatial and statistical distribution of standardized inland water N_2O emission flux. Regional estimates of N_2O emission (Gg N_2O yr^{-1}) in the top bars, ice corrected surface area estimates in blue lines, and the percent change in total annual emission from the combination of ice and ice melt corrections in the bottom bars. Regional emissions are shown from rivers (dark blue), natural lakes (light blue), reservoirs (green) and lakes with a dam (yellow). Each black dot represents the regionalized emission from one study in the literature, such that the bars show the range of regionalized emissions across studies. More details on the individual values can be found in Table S1.

6 Overall inland water GHG budget

To compare estimates of inland water GHG emissions across different gas types, emissions were expressed as CO_2 equivalents. Using the emission conversion factors recommended by the IPCC AR6, we have calculated the CO_2 equivalents for a 20 year and 100 year horizon. At the 100 year horizon, 1 kg of CH_4 or N_2O have the same global warming potential (GWP_{100}) as 27 or 273 kg CO_2, respectively. At the 20 year horizon, which is more relevant for projections until the middle of this century, the global warming potential (GWP_{20}) of 1 kg of CH_4 reaches that of 81 kg CO_2. This difference is due to the half-life time of CH_4 of 9.1 years. On the other hand, partly due to its long half-life (114 years), the N_2O warming potential at the 20 year horizon is not different from that at the 100 year horizon.

Further, when combining the estimates for different GHGs and different types of inland waters, a large number of alternative combinations of individual estimates are again possible. First, we simply combined

median flux estimates per GHG, inland water type and RECCAP-2 region, which were then summed up to obtain a best estimate of global fluxes. We then added the interquartile range (IQR) from all possible combinations of emission estimates per type of inland water, GHG and RECCAP-2 region as bounds to these median estimates. This yielded global inland water emissions with a GWP_{20} and GWP_{100} of 13.6 (10.0-20.3) and 8.3 (5.8-12.7) Pg CO_2-eq. yr^{-1}, respectively (Figure 5, Table 1).

Considering median estimates, rivers are responsible for more than half (63%) of the GWP_{100} of global inland water GHG emissions, with a dominant contribution from CO_2 (87%) and a minor contribution from CH_4 (12%) (Fig. 5a, Table 1). About one third (29%) of total emissions can be attributed to natural lakes (LT1), with minor contributions from reservoirs (LT2, 5%) and lakes regulated by dams (LT3, 3%). In contrast to rivers, for each of the three lake types, CH_4 accounts for more than two thirds of the GWP_{100}, corroborating earlier global scale assessments by Deemer et al. (2016) and DelSontro et al. (2018). At a 20 year horizon, the contributions of CH_4 emissions are substantially higher as a result of the higher conversion factor. It even becomes the dominant contributor to GWP_{20} before CO_2 with 60% vs. 40%, respectively, while it contributes only 33% to GWP_{100} (Fig. 5b, Table 1). Due to the higher weight of CH_4 emissions in GWP_{20}, lakes are a similarly important contributor to GWP_{20} compared to rivers. Most surprisingly, the contribution of inland water N_2O emissions are negligible at both time horizons, in line with previous findings from a regional budget for African inland waters (Borges et al. 2015) and from a global assessment of reservoir emissions alone (Deemer et al. 2016).

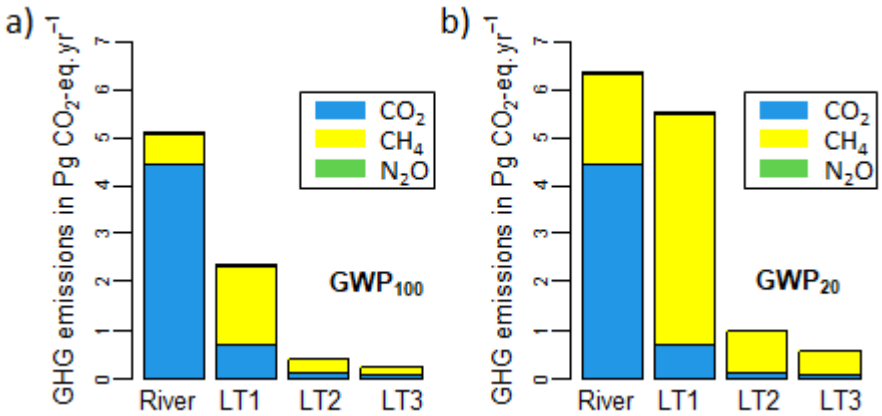

Figure 5: Warming potential of global inland water greenhouse gas emissions based on the medians of rescaled estimates, distinguishing contributions from rivers and three types of lakes (LT): natural lakes (LT1), reservoirs (LT2) and lakes regulated by dams (LT3). The warming potential is expressed as CO_2-equivalents at **a)** 100 year and **b)** 20 year time horizons.

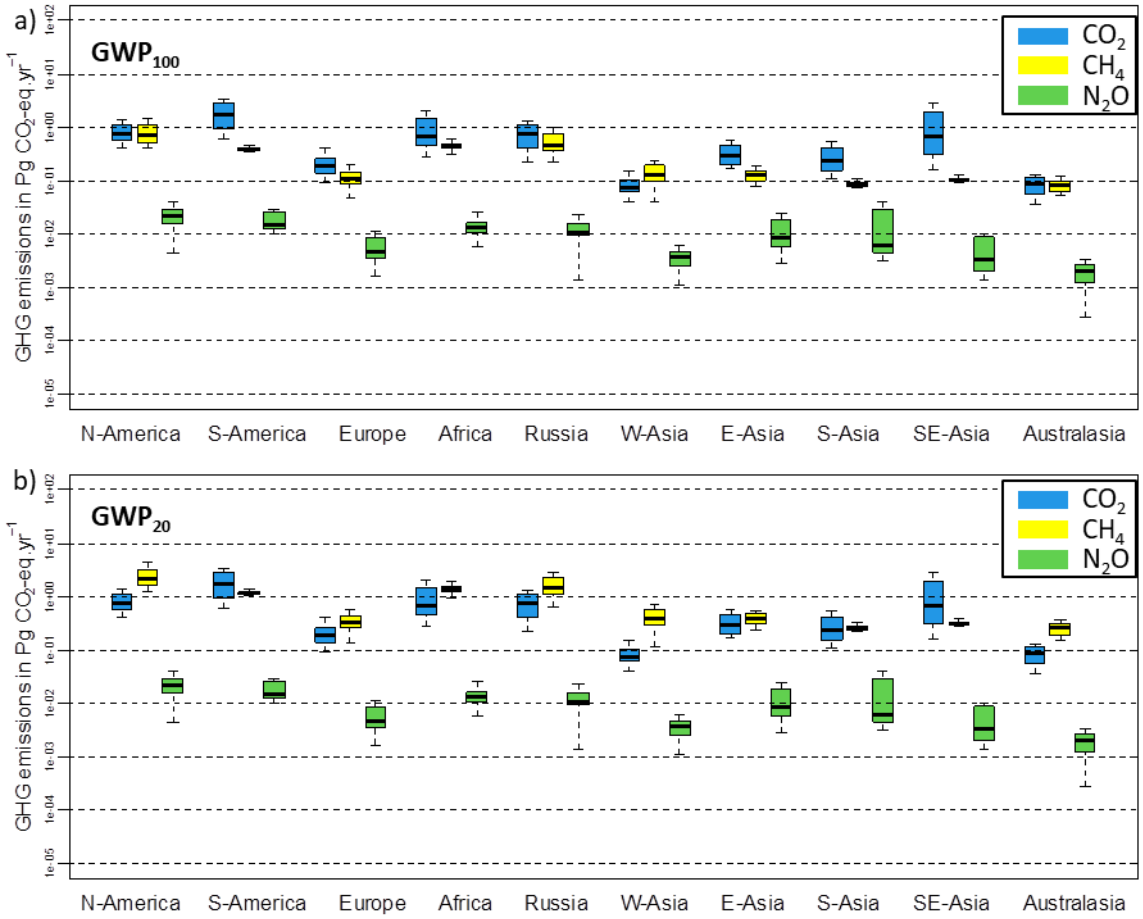

Figure 6: Spatial and statistical distribution of Global Warming Potentials (GWPs) of standardized inland water GHG emissions. Regional estimates of CO_2, CH_4, and N_2O, expressed as CO_2 equivalents at the **a)** 100 year and **b)** 20 year horizon. The boxplots represent median, interquartile range and total range of rescaled estimates per RECCAP-2 region.

Figure 6 shows the statistical distribution of the rescaled estimates for each of the three GHGs and the ten RECCAP-2 regions. The most important regional contributors to the GWP_{20} and GWP_{100} of global inland water GHG emissions are N- and S-America, followed by Russia and Africa (Table 1). These four regions together contribute about three quarters to the GWPs of global inland water emissions. That ranking is however heavily influenced by the areal extent of each RECCAP-2 region. If we normalize emissions by the area of RECCAP-2 regions, we identify the highest CO_2-equivalent emission rates for SE-Asia, followed by S-America and Russia (Table 1). Rivers are the dominant contributors to GWPs of inland water emissions in S-America and SE-Asia, while in N-America and Russia lakes have a much higher weight.

From the range of estimates reported in Figure 6, we see once again that inland water N_2O emissions are the least well constrained. However, based on the ensemble of estimates, the contribution of N_2O to the GWP of inland water GHG emissions seems to be negligible in most areas of the world. CO_2 is the largest contributor to the GWP_{100} of inland water GHG emissions in S-America, S-, E- and SE-Asia. On the

contrary, contributions of CH_4 to GWP_{100} of inland water emissions are higher than that of CO_2 in N-America, W-Asia, and Australasia (Table 1). The relative contribution of CH_4 is clearly linked to the contribution of lakes to the inland water emissions (Table 1), for which the proportion of CH_4 in the overall GWPs is much higher than for rivers (Figure 5). For GWP_{20}, for which the relative weight of CH_4 is stronger, CH_4 appears to be the most important contributor for eight of the ten RECCAP-2 regions (Table 1). The two exceptions, S-America and SE-Asia, are strongly dominated by emissions from rivers and thus also by emissions of CO_2.

Table 1: Global warming potential at 20 (GWP_{20}) and 100 (GWP_{100}) year horizons. Emissions are given as the median (interquartile range) of CO_2 equivalents. Relative contribution per gas and inland water type refer to median estimates.

GWP20

RECCAP2 zone		Total emissions (median [IQ range])		Contribution per gas [%]			Contribution per inland water type [%]			
No	Name	Tg $CO_{2\text{-eq.}}$/yr	g $CO_{2\text{-eq}}/m^2/yr$*	CO_2	CH_4	N_2O	Rivers	LT1	LT2	LT3
1	N-America	2,877 (2,131-4,553)	119 (88-188)	24	75	1	16	71	8	5
2	S-America	2,872 (2,140-3,813)	161 (120-214)	59	40	0	80	13	7	0
3	Europe	518 (413-727)	87 (69-122)	34	66	1	34	48	10	9
4	Africa	2,088 (1,602-3,048)	69 (53-101)	32	67	1	47	31	9	13
5	Russia	2,219 (1,510-3,547)	131 (89-210)	35	65	0	33	59	4	4
6	W-Asia	466 (361-696)	43 (34-65)	15	84	1	11	78	8	3
7	E-Asia	687 (479-991)	59 (41-86)	43	56	1	52	38	9	1
8	S-Asia	510 (402-676)	114 (90-151)	48	51	1	77	8	15	0
9	SE-Asia	1,021 (683-1,800)	202 (135-356)	68	31	0	87	9	3	1
10	Australia	344 (238-419)	43 (30-52)	24	76	1	27	66	6	2
	Global	13,605 (9,959-20,268)	101 (74-150)	40	60	1	47	41	7	4

GWP100

RECCAP2 zone		Total emissions (median [IQ range])		Contribution per gas [%]			Contribution per inland water type [%]			
No	Name	Tg $CO_{2\text{-eq.}}$/yr	g $CO_{2\text{-eq}}/m^2/yr$*	CO_2	CH_4	N_2O	Rivers	LT1	LT2	LT3
1	N-America	1,445 (1,164-,2174)	60 (48-90)	49	50	2	26	63	7	4
2	S-America	2,106 (1,401-2,994)	118 (78-168)	81	18	1	88	8	4	0
3	Europe	310 (226-413)	52 (38-69)	60	39	2	48	38	7	7
4	Africa	1,149 (891-2,055)	38 (30-68)	58	41	1	63	22	6	9
5	Russia	1,296 (785-1,896)	77 (46-112)	61	38	1	48	45	3	3
6	W-Asia	209 (169-288)	19 (16-27)	35	63	2	19	70	8	3
7	E-Asia	436 (303-647)	38 (26-56)	69	29	2	68	25	7	1
8	S-Asia	340 (250-478)	76 (56-107)	73	26	2	85	5	10	0
9	SE-Asia	807 (484-1,577)	160 (96-312)	86	13	0	93	5	2	0
10	Australia	169 (125-216)	21 (16-27)	48	51	1	44	51	5	1
	Global	8,268 (5,796-12,738)	61 (43-94)	66	33	1	63	29	5	3

*global warming potential of inland water emissions expressed as rates of CO_2 equivalents normalized by the total area (terrestrial+wetland+inland water) of each RECCAP-2 region.

**Inland water types considered in this study: Rivers (all flowing waters including from small headwater streams to large rivers) and three lake types (LT) – LT1 = natural lakes, LT2 = reservoirs, LT3 = lakes regulated by a dam

7 Conclusions and outlook

From our synthesis of inland water GHG emission estimates, we obtained estimates of global CO_2 emissions of 5.6 (IQR: 3.5-9.1) Pg CO_2 yr^{-1}, which are comparable to the values obtained in RECCAP-1 (Raymond et al., 2013). In contrast, our synthesized global estimates for CH_4 (101, IQR: 83-135 Tg CH_4 yr^{-1}) and N_2O (326, IQR: 254-592 Gg N_2O yr^{-1}) emissions fall on the lower end of the range of estimates reported in AR6 of the IPCC. We find remarquable differences in the contributions of rivers, lakes, and reservoirs, and of the ten RECCAP-2 regions to global inland water GHG emissions. South-American rivers contribute about one third of global inland water CO_2 emissions. North-American and Russian lakes contribute together one third of global inland water CH_4 emissions. And finally, North America alone contributes one fourth of global inland water N_2O emissions.

Our synthesis suggests that global inland water GHG emissions have a GWP of 8.3 (IQR: 5.8-12.7) or 13.6 (IQR: 10.0-20.3) Pg $CO_{2\text{-eq}}$. yr^{-1} at a 100 or 20 year horizon, respectively. In terms of GWP, inland water emissions of CO_2 and CH_4 are of similar importance, with CO_2 dominating emissions from rivers and CH_4 dominating emissions from lakes, while contributions from N_2O seem by far less important for any type of inland waters. In addition, inland water emissions have a different importance for the overall continental budgets of CO_2, CH_4, and N_2O. While inland water N_2O emissions already appear rather small compared to emissions of CO_2 and CH_4, their contribution to the global N_2O budget appears also negligible. Our synthesized estimate does not represent more than 1% of global emission of 53 Tg N_2O yr^{---1} synthesized in the first global N_2O budget of the Global Carbon Project (GCP) (Tian et al., 2020). But also inland water CO_2 emissions, which are important in terms of GWP and total flux in the overall GHG budget of inland waters, are relatively small compared to other flux components of the continental CO_2 budget. Being mostly fed by autotrophic and heterotrophic respiration in upland soils, wetlands and aquatic systems (Abril & Borges, 2019; Battin et al. in rev.), it is fair to consider inland water CO_2 emissions as a fraction of continental ecosystem respiration. Our synthesized estimate of global inland water CO_2 emissions would represent only about 1-2% of continental ecosystem respiration (cf. Battin et al. in rev, Ciais et al., 2021), a proportion much lower than the uncertainties related to the quantification of this flux at global scale. However, inland water emissions are in the order of magnitude of net-CO_2 uptake by terrestrial ecosystems (land C sink minus LUC emissions, Friedlingstein et al., 2020), and should thus be represented in detailed CO_2 budgets. Dynamic global vegetation models (DGVMs) simulate CO_2 budgets of continental ecosystems while ignoring aquatic C cycling (Ciais et al, 2021). However, those models may simply compensate for this missing flux of inland water CO_2 emissions by a slightly higher soil respired CO_2 emission flux, while biases in simulated land CO_2 uptake may rather be linked to the non-representation of lateral C exports to the coast (Lauerwald et al., 2020). Also global scale atmospheric inversions usually do not consider inland waters as a specific source of emissions, because it is not possible to separate terrestrial and aquatic signals due to the coarse resolution of inversions and the relatively small size of most inland waters. In contrast, estimates of terrestrial CO_2 budgets upscaled from flux tower measurements (e.g. FLUXCOM, Jung et al., 2020), which focus more explicitly on terrestrial ecosystems or wetlands, will not account for inland water emissions, and would need to be complemented with corresponding estimates.

In contrast to CO_2 and N_2O, global inland water CH_4 emissions could easily represent ~20% of global total emissions of 576 Tg CH_4 yr^{-1} estimated from atmospheric inversion in the most recent global methane budget by Saunois et al. (2020). The potential importance of inland water CH_4 emissions is even higher if compared to the top-down estimate of only natural emissions of 218 Tg CH_4 yr^{-1} (Saunois et al. 2020). In the global methane budget of the Global Carbon Project, inland water CH_4 emissions are grouped into the category "other natural emissions", together with emissions from geologic sources, termites, vegetation, oceans, wild animals and permafrost. This category complements "wetlands" as a major natural source of CH_4. Interestingly, bottom-up estimates of these "other natural emissions" are much higher than the corresponding estimates based on atmospheric inversions, with 222 (143-306) Tg CH_4 yr^{-1} vs. 37 (21-50) Tg CH_4 yr^{-1} (mean and range, Saunois et al. 2020). Thus, the estimates from our synthesis seem rather high if compared to this top-down estimate. In contrast to this, in the same budget, bottom-up estimates tend to be lower than top-down estimates for "wetland emissions" with 149 (102-182) vs. 182 (159-200) Tg CH_4 yr^{-1} (mean and range, Saunois et al. 2020). As wetlands and inland waters may be spatially correlated at regional to global scales, it is difficult to distinguish both sources in inversions. Thus, it may be possible that wetlands as methane source may have been overestimated to the detriment of inland water sources. More systematic investigations of CH_4 emissions from upland, wetland and aquatic ecosystems will be needed to clarify what causes the mismatch between top-down and bottom up estimates, and to more accurately separate wetland from aquatic emissions of CH_4.

One of the greatest weaknesses of our synthesis is the non-representation of smallest standing water bodies with an area < 0.1 km^2 and which may contribute substantially to CH_4 and CO_2 emissions. These water bodies were neglected because reliable datasets on geographic distribution, size and classification of small water bodies are not available yet. In addition, more data on emission rates, including CH_4 ebullition, are required. Our estimates of total inland water GHG emissions are thus still likely conservative. Future estimates should try to include these smaller water bodies, which may make separation between wetland and aquatic systems further challenging. Along the same lines, there are certain types of small wetlands, like fringing lacustrine and riverine wetlands, which are not included in this study, and which are not yet included in any global wetland GHG assessment. Same is true for ephemeral water bodies, which are also not included in our synthesis. While this synthesis effort presented here is an important step forward in including inland waters in regionalised GHG budgets, future research has to invest more efforts into the consistent integration of GHG budgets of inland water, wetland and terrestrial ecosystems.

Acknowledgements

Any use of trade, firm, or product names is for descriptive purposes only and does not imply endorsement by the US Government. Ronny Lauerwald acknowledges funding from French state aid, managed by ANR under the "Investissements d'avenir" programme (ANR-16-CONV-0003). George Allen was funded by a US National Science Foundation CAREER Award (grant no: EAR 2145628). Shaoda Liu was funded by the National Key Research and Development Program of China (2021YFC3200401). Matthew Johnson was funded for this work by NASA's Interdisciplinary Research in Earth Science (IDS) Program and the NASA Terrestrial Ecology and Tropospheric Composition Programs. Adam Hastie was funded by NERC (grant ref. NE/R000751/1). David Bastviken was funded by the European Research

Council (ERC; grant agreement No 725546; METLAKE), the Swedish Research Council (grant No 2016-04829), and FORMAS (grant No 2018-01794). Meredith Holgerson was funded by a US National Science Foundation CAREER Award (grant no: DEB 2143449). Pierre Regnier acknowledges funding from the European Union's Horizon 2020 research and innovation program under grant agreement no. 101003536 (ESM2025 – Earth System Models for the Future). Alessandra Marzadri acknowledges funding from the Italian Ministry of Education, University and Research (MIUR) in the frame of the Departments of Excellence Initiative 2018-2022. Lishan Ran was funded by the Research Grants Council of Hong Kong (grant No 17300621). Hanqn Tian acknowledges funding from US National Science Foundation award (grant no. 1903722).

Literature

Abril, G., & Borges, A. V. (2019). Ideas and perspectives: Carbon leaks from flooded land: do we need to replumb the inland water active pipe? *Biogeosciences*, *16*(3), 769–784. https://doi.org/10.5194/bg-16-769-2019

Allen, G. H., & Pavelsky, T. (2018). Global extent of rivers and streams. *Science*, *361*(6402), 585–588. https://doi.org/10.1126/science.aat063

Allen, P. M., Arnold, J. C., & Byars, B. W. (1994). Downstream channel geometry for use in planning-level models. *JAWRA Journal of the American Water Resources Association*, *30*(4), 663–671. https://doi.org/10.1111/j.1752-1688.1994.tb03321.x

Aufdenkampe, A. K., Mayorga, E., Raymond, P. A., Melack, J. M., Doney, S. C., Alin, S. R., et al. (2011). Riverine coupling of biogeochemical cycles between land, oceans, and atmosphere. *Frontiers in Ecology and the Environment*, *9*(1), 53–60. https://doi.org/10.1890/100014

Bastos, A., O'Sullivan, M., Ciais, P., Makowski, D., Sitch, S., Friedlingstein, P., et al. (2020). Sources of Uncertainty in Regional and Global Terrestrial CO2 Exchange Estimates. *Global Biogeochemical Cycles*, *34*(2). https://doi.org/10.1029/2019GB006393

Bastviken, David, Tranvik, L. J., Downing, J. A., Crill, P. M., & Enrich-Prast, A. (2011). Freshwater Methane Emissions Offset the Continental Carbon Sink. *Science*, *331*(6013), 50–50. https://doi.org/10.1126/science.1196808

Borges, Alberto V., Darchambeau, F., Teodoru, C. R., Marwick, T. R., Tamooh, F., Geeraert, N., et al. (2015). Globally significant greenhouse-gas emissions from African inland waters. *Nature Geoscience*, *8*(8), 637–642. https://doi.org/10.1038/ngeo2486

Butman, D., & Raymond, P. A. (2011). Significant efflux of carbon dioxide from streams and rivers in the United States. *Nature Geoscience*, *4*(12), 839–842. https://doi.org/10.1038/ngeo1294

Cavaliere, E., & Baulch, H. M. (2018). Denitrification under lake ice. *Biogeochemistry*, *137*(3), 285–295. https://doi.org/10.1007/s10533-018-0419-0

Chu, H., Luo, X., Ouyang, Z., Chan, W. S., Dengel, S., Biraud, S. C., et al. (2021). Representativeness of Eddy-Covariance flux footprints for areas surrounding AmeriFlux sites. *Agricultural and Forest Meteorology*, *301–302*, 108350. https://doi.org/10.1016/j.agrformet.2021.108350

Ciais, P., Yao, Y., Gasser, T., Baccini, A., Wang, Y., Lauerwald, R., et al. (2021). Empirical estimates of regional carbon budgets imply reduced global soil heterotrophic respiration. *National Science Review*, *8*(2). https://doi.org/10.1093/nsr/nwaa145

Ciais, P., Bastos, A., Chevallier, F., Lauerwald, R., Poulter, B., Canadell, P., et al. (2022). Definitions and methods to estimate regional land carbon fluxes for the second phase of the REgional Carbon Cycle Assessment and Processes Project (RECCAP-2). *Geoscientific Model Development*, *15*(3), 1289–1316. https://doi.org/10.5194/gmd-15-1289-2022

Cole, J. J., Prairie, Y. T., Caraco, N. F., McDowell, W. H., Tranvik, L. J., Striegl, R. G., et al. (2007). Plumbing the Global Carbon Cycle: Integrating Inland Waters into the Terrestrial Carbon Budget. *Ecosystems*, *10*(1), 172–185. https://doi.org/10.1007/s10021-006-9013-8

Deemer, B. R., Harrison, J. A., Li, S., Beaulieu, J. J., DelSontro, T., Barros, N., et al. (2016). Greenhouse Gas Emissions from Reservoir Water Surfaces: A New Global Synthesis. *BioScience*, *66*(11), 949–964. https://doi.org/10.1093/biosci/biw117

DelSontro, T., Beaulieu, J. J., & Downing, J. A. (2018). Greenhouse gas emissions from lakes and impoundments: Upscaling in the face of global change. *Limnology and Oceanography Letters*, *3*(3), 64–75. https://doi.org/10.1002/lol2.10073

Denfeld, B. A., Baulch, H. M., del Giorgio, P. A., Hampton, S. E., & Karlsson, J. (2018). A synthesis of carbon dioxide and methane dynamics during the ice-covered period of northern lakes. *Limnology and Oceanography Letters*, *3*(3), 117–131. https://doi.org/10.1002/lol2.10079

Fick, S. E., & Hijmans, R. J. (2017). WorldClim 2: new 1-km spatial resolution climate surfaces for global land areas. *International Journal of Climatology*, *37*(12), 4302–4315. https://doi.org/10.1002/joc.5086

Friedlingstein, P., O'Sullivan, M., Jones, M. W., Andrew, R. M., Hauck, J., Olsen, A., et al. (2020). Global Carbon Budget 2020. *Earth Syst. Sci. Data*, *12*(4), 3269–3340. https://doi.org/10.5194/essd-12-3269-2020

Harrison, John A., Prairie, Y. T., Mercier-Blais, S., & Soued, C. (2021). Year-2020 Global Distribution and Pathways of Reservoir Methane and Carbon Dioxide Emissions According to the Greenhouse Gas From Reservoirs (G-res) Model. *Global Biogeochemical Cycles*, *35*(6), e2020GB006888. https://doi.org/10.1029/2020GB006888

Hastie, A., Lauerwald, R., Weyhenmeyer, G., Sobek, S., Verpoorter, C., & Regnier, P. (2018). CO2 evasion from boreal lakes: Revised estimate, drivers of spatial variability, and future projections. *Global Change Biology*, *24*(2), 711–728. https://doi.org/10.1111/gcb.13902

Holgerson, M. A., & Raymond, P. A. (2016). Large contribution to inland water CO2 and CH4 emissions from very small ponds. *Nature Geoscience*, *9*(3), 222–226. https://doi.org/10.1038/ngeo2654

Horgby, Å., Segatto, P. L., Bertuzzo, E., Lauerwald, R., Lehner, B., Ulseth, A. J., et al. (2019). Unexpected large evasion fluxes of carbon dioxide from turbulent streams draining the world's mountains. *Nature Communications*, *10*(1). https://doi.org/10.1038/s41467-019-12905-z

Hu, M., Chen, D., & Dahlgren, R. A. (2016). Modeling nitrous oxide emission from rivers: a global assessment. *Global Change Biology*, *22*(11), 3566–3582. https://doi.org/10.1111/gcb.13351

Johnson, Matthew S., Matthews, E., Bastviken, D., Deemer, B., Du, J., & Genovese, V. (2021). Spatiotemporal Methane Emission From Global Reservoirs. Journal of Geophysical Research: Biogeosciences, 126(8), e2021JG006305. https://doi.org/10.1029/2021JG006305

Johnson, M.S., Matthews, E., Du, J., Genovese, V., & Bastviken, D. (2022). Methane Emission From Global Lakes: New Spatiotemporal Data and Observation-Driven Modeling of Methane Dynamics Indicates Lower Emissions. Journal of Geophysical Research: Biogeosciences, 127(7). https://doi.org/10.1029/2022JG006793

Jung, M., Schwalm, C., Migliavacca, M., Walther, S., Camps-Valls, G., Koirala, S., et al. (2020). Scaling carbon fluxes from eddy covariance sites to globe: synthesis and evaluation of the FLUXCOM approach. *Biogeosciences*, *17*(5), 1343–1365. https://doi.org/10.5194/bg-17-1343-2020

Kuhn, M. A., Varner, R. K., Bastviken, D., Crill, P., MacIntyre, S., Turetsky, M., et al. (2021). BAWLD-CH4: a comprehensive dataset of methane fluxes from boreal and arctic ecosystems. *Earth Syst. Sci. Data*, *13*(11), 5151–5189. https://doi.org/10.5194/essd-13-5151-2021

Lauerwald, R., Laruelle, G. G., Hartmann, J., Ciais, P., & Regnier, P. A. G. (2015). Spatial patterns in CO2 evasion from the global river network. *Global Biogeochemical Cycles*, *29*(5), 534–554. https://doi.org/10.1002/2014GB004941

Lauerwald, R., Regnier, P., Camino-Serrano, M., Guenet, B., Guimberteau, M., Ducharne, A., et al. (2017). ORCHILEAK (revision 3875): A new model branch to simulate carbon transfers along the terrestrial-aquatic continuum of the Amazon basin. *Geoscientific Model Development*, *10*(10), 3821–3859. https://doi.org/10.5194/gmd-10-3821-2017

Lauerwald, R., Regnier, P., Figueiredo, V., Enrich-Prast, A., Bastviken, D., Lehner, B., et al. (2019). Natural Lakes Are a Minor Global Source of N2O to the Atmosphere. *Global Biogeochemical Cycles*, *33*(12), 1564–1581. https://doi.org/10.1029/2019GB006261

Lauerwald, R., Regnier, P., Guenet, B., Friedlingstein, P., & Ciais, P. (2020). How Simulations of the Land Carbon Sink Are Biased by Ignoring Fluvial Carbon Transfers: A Case Study for the Amazon Basin. *One Earth*, *3*(2), 226–236. https://doi.org/10.1016/j.oneear.2020.07.009

Li, S., Bush, R. T., Santos, I. R., Zhang, Q., Song, K., Mao, R., et al. (2018). Large greenhouse gases emissions from China's lakes and reservoirs. *Water Research*, *147*, 13–24. https://doi.org/10.1016/j.watres.2018.09.053

Linke, S., Lehner, B., Ouellet Dallaire, C., Ariwi, J., Grill, G., Anand, M., et al. (2019). Global hydro-environmental sub-basin and river reach characteristics at high spatial resolution. *Scientific Data*, *6*(1), 283. https://doi.org/10.1038/s41597-019-0300-6

Liu, S., Kuhn, C., Amatulli, G., Aho, K., Butman, D. E., Allen, G. H., et al. (2022). The importance of hydrology in routing terrestrial carbon to the atmosphere via global streams and rivers.

Proceedings of the National Academy of Sciences, *119*(11), e2106322119. https://doi.org/10.1073/pnas.2106322119

Maavara, T., Lauerwald, R., Laruelle, G. G., Akbarzadeh, Z., Bouskill, N. J., Van Cappellen, P., & Regnier, P. (2019). Nitrous oxide emissions from inland waters: Are IPCC estimates too high? *Global Change Biology*, *25*(2), 473–488. https://doi.org/10.1111/gcb.14504

Marzadri, A., Amatulli, G., Tonina, D., Bellin, A., Shen, L. Q., Allen, G. H., & Raymond, P. A. (2021). Global riverine nitrous oxide emissions: The role of small streams and large rivers. *Science of The Total Environment*, *776*, 145148. https://doi.org/10.1016/j.scitotenv.2021.145148

Messager, M.L., Lehner, B., Grill, G., Nedeva, I., & Schmitt, O. (2016). Estimating the volume and age of water stored in global lakes using a geo-statistical approach. *Nature Communications*, *7*. https://doi.org/10.1038/ncomms13603

Murfitt, J., & Brown, L. C. (2017). Lake ice and temperature trends for Ontario and Manitoba: 2001 to 2014. *Hydrological Processes*, *31*(21), 3596–3609. https://doi.org/10.1002/hyp.11295

Ran, L., Butman, D. E., Battin, T. J., Yang, X., Tian, M., Duvert, C., et al. (2021). Substantial decrease in CO2 emissions from Chinese inland waters due to global change. *Nature Communications*, *12*(1), 1730. https://doi.org/10.1038/s41467-021-21926-6

Raymond, P.A., Hartmann, J., Lauerwald, R., Sobek, S., McDonald, C., Hoover, M., et al. (2013). Global carbon dioxide emissions from inland waters. *Nature*, *503*(7476), 355–359. https://doi.org/10.1038/nature12760

Rosentreter, J. A., Borges, A. V., Deemer, B. R., Holgerson, M. A., Liu, S., Song, C., et al. (2021). Half of global methane emissions come from highly variable aquatic ecosystem sources. *Nature Geoscience*, *14*(4), 225–230. https://doi.org/10.1038/s41561-021-00715-2

Saunois, M., Stavert, A. R., Poulter, B., Bousquet, P., Canadell, J. G., Jackson, R. B., et al. (2020). The Global Methane Budget 2000–2017. *Earth Syst. Sci. Data*, *12*(3), 1561–1623. https://doi.org/10.5194/essd-12-1561-2020

Sharma, S., Blagrave, K., Magnuson, J. J., O'Reilly, C. M., Oliver, S., Batt, R. D., et al. (2019). Widespread loss of lake ice around the Northern Hemisphere in a warming world. *Nature Climate Change*, *9*(3), 227–231. https://doi.org/10.1038/s41558-018-0393-5

Soued, C., del Giorgio, P. A., & Maranger, R. (2016). Nitrous oxide sinks and emissions in boreal aquatic networks in Québec. *Nature Geoscience*, *9*(2), 116–120. https://doi.org/10.1038/ngeo2611

St. Louis, V. L., Kelly, C. A., Duchemin, É., Rudd, J. W. M., & Rosenberg, D. M. (2000). Reservoir Surfaces as Sources of Greenhouse Gases to the Atmosphere: A Global Estimate: Reservoirs are sources of greenhouse gases to the atmosphere, and their surface areas have increased to the point where they should be included in global inventories of anthropogenic emissions of greenhouse gases. *BioScience*, *50*(9), 766–775. https://doi.org/10.1641/0006-3568(2000)050[0766:RSASOG]2.0.CO;2

Stanley, E. H., Casson, N. J., Christel, S. T., Crawford, J. T., Loken, L. C., & Oliver, S. K. (2016). The ecology of methane in streams and rivers: patterns, controls, and global significance. *Ecological Monographs*, *86*(2), 146–171. https://doi.org/10.1890/15-1027

Stavert, A. R., Saunois, M., Canadell, J. G., Poulter, B., Jackson, R. B., Regnier, P., et al. (2022). Regional trends and drivers of the global methane budget. *Global Change Biology*, *28*(1), 182–200. https://doi.org/10.1111/gcb.15901

Tian, H., Xu, R., Canadell, J. G., Thompson, R. L., Winiwarter, W., Suntharalingam, P., et al. (2020). A comprehensive quantification of global nitrous oxide sources and sinks. *Nature*, *586*(7828), 248–256. https://doi.org/10.1038/s41586-020-2780-0

Tian, H., W. Ren, J. Yang, B.Tao, W. Cai, S. E. Lohrenz, C.S. Hopkinson, M. Liu, Q. Yang, C. Lu, B. Zhang, K. Banger, S. Pan, R. He and Z. Xue (2015). Climate extremes dominating seasonal and interannual variations in carbon export from the Mississippi River Basin, *Global Biogeochem. Cycles*, 29 (9), 1333-1347, DOI: 10.1002/2014GB005068

Tranvik, L. J., Downing, J. A., Cotner, J. B., Loiselle, S. A., Striegl, R. G., Ballatore, T. J., et al. (2009). Lakes and reservoirs as regulators of carbon cycling and climate. *Limnology and Oceanography*, *54*(6part2), 2298–2314. https://doi.org/10.4319/lo.2009.54.6_part_2.2298

Verpoorter, C., Kutser, T., Seekell, D. A., & Tranvik, L. J. (2014). A global inventory of lakes based on high-resolution satellite imagery. *Geophysical Research Letters*, *41*(18), 6396–6402. https://doi.org/10.1002/2014GL060641

Weyhenmeyer, G. A., Meili, M., & Livingstone, D. M. (2004). Nonlinear temperature response of lake ice breakup. *Geophysical Research Letters*, *31*(7), L07203 1-4. https://doi.org/10.1029/2004GL019530

Wik, M., Varner, R. K., Anthony, K. W., MacIntyre, S., & Bastviken, D. (2016). Climate-sensitive northern lakes and ponds are critical components of methane release. *Nature Geoscience*, *9*(2), 99–105. https://doi.org/10.1038/ngeo2578

Yang, X., Pavelsky, T. M., & Allen, G. H. (2020). The past and future of global river ice. *Nature*, *577*(7788), 69–73. https://doi.org/10.1038/s41586-019-1848-1

Yao, Y., Tian, H., Shi, H., Pan, S., Xu, R., Pan, N., & Canadell, J. G. (2020). Increased global nitrous oxide emissions from streams and rivers in the Anthropocene. *Nature Climate Change*, *10*(2), 138–142. https://doi.org/10.1038/s41558-019-0665-8